Using Horizontal to Vertical Spectral Ratios to construct shear-wave velocity profiles

Janneke van Ginkel[1,2], Elmer Ruigrok[1,3], and Rien Herber[1]

[1]Energy and Sustainability Research Institute Groningen, University of Groningen, Nijenborgh 6, 9747 AG Groningen, the Netherlands.
[2]R&D Seismology and Acoustics, Royal Netherlands Meteorological Institute, Utrechtseweg 297, 3731 GA De Bilt, the Netherlands.
[3]Department of Earth Sciences, Utrecht University, Princetonlaan 8a, 3584 CB Utrecht, the Netherlands

Correspondence: Janneke van Ginkel (j.a.van.ginkel@rug.nl)

Abstract. For hazard assessment and earthquake hypocentre localisation, detailed shear-wave velocity profiles are an important input parameter. Here we present a method to construct a shear-wave velocity profiles for a deep unconsolidated sedimentary layer by using strong teleseismic phases and the ambient noise field. Gas extraction in the Groningen field, in the northern part of the Netherlands, is causing low-magnitude, induced seismic events. This region forms an excellent case study due to the presence of a permanent borehole network and detailed subsurface knowledge. Instead of conventional horizontal-to-vertical spectral ratios (H/V ratios) from amplitude spectra, we calculate power spectral densities and use those as input for H/V calculations. The strong teleseisms provide resonance recordings at low frequencies, where the seismic noise field is too weak to be recorded well with the employed geophones and accelerometers. The H/V ratios of the ambient noise field are compared with several forward modeling approaches to quality check the teleseism-based shear-wave velocity profiles. A close relationship is observed between the H/V spectral ratios from the ambient noise field, shear-wave resonance frequencies and Rayleigh-wave ellipticity. Using the well-constrained depth of the sedimentary basin, we invert the H/V ratios for velocity profiles. By processing only five teleseismic events, we are able to derive shear-wave velocities for the deeper sedimentary sequence with a 7% bias in comparison with the existing detailed velocity model for the Cenozoic sediments overlying the Groningen gas field. Furthermore, a relation between resonance frequency and unconsolidated sediment thickness is derived, to be used in other areas in the Netherlands, where detailed depth maps are not available.

1 Introduction

Induced earthquakes in the province of Groningen, the Netherlands, are caused by reservoir compaction due to exploitation of the large gas field. Since 2003, the number of seismic events and the magnitudes started to increase (van Thienen-Visser and Breunese, 2015) and subsequently triggered the research on induced earthquakes and site response in the Netherlands

(Bommer et al., 2017, 2016; Rodriguez-Marek et al., 2017; Noorlandt et al., 2018; Kruiver et al., 2017). Although the magnitudes of the earthquakes recorded to date are relatively small (maximum magnitude of 3.6), damage on houses is significant, amongst other due to the shallow depth of the events (approximately 3 km). An extra factor leading to significant damage of these low-magnitude earthquakes is the presence of a low-velocity sedimentary cover. A soft sedimentary cover has a strong effect on seismic wave propagation and these effects have been observed and studied after multiple occurrences, e.g. after the Mexico City earthquake in 1985 (Bard et al., 1988) and the Darfield earthquake in 2010, New Zealand (Bradley, 2012). Since the installation of a borehole seismic network in Groningen in 2015 (Fig. 2), a region-specific ground-motion prediction model has been developed, including the effect of the sedimentary cover on wave propagation (Bommer et al., 2016, 2017; Rodriguez-Marek et al., 2017; Noorlandt et al., 2018). This study aims to present a method to constrain the shear-wave velocities of the sedimentary cover, specifically for each borehole location. Moreover, we use the rich Groningen dataset to fit a function between resonance frequency and sediment depth, to be used in settings with a similar Cenozoic sedimentary cover, but where basin depth is poorly known.

Seismic properties of the subsurface can be estimated through the use of the ambient noise field or microtremors. Many experiments established that the H/V spectral ratio (the ratio between the amplitude spectra of the horizontal and vertical component of a seismic recording) shows a correlation with the fundamental resonance frequency of the recording site (Arai and Tokimatsu, 2005; Bonnefoy-Claudet et al., 2006a; Fäh et al., 2001; Lermo and Chavez-Garcia, 1993; Nakamura, 1989, 2019; Scherbaum et al., 2003; Parolai et al., 2002). More recently, also teleseismic phases are used to study the resonance of deep sedimentary basins (Nishitsuji et al., 2014; Ruigrok et al., 2012). The H/V method is based on the assumption that when a strong interface between bedrock and soft sediments is present, the peak in the H/V curve is closely related to the shear-wave resonance frequency for that site. Based on the knowledge of the fundamental resonance frequency and layer thickness, one can determine constraints on the shear-wave velocity structure (Arai and Tokimatsu, 2004; Fäh et al., 2003; Parolai et al., 2002; Scherbaum et al., 2003; Tsai and Housner, 1970). Zhu et al. (2020) presented an overview of the uncertainties of using Fourier amplitude spectra or response spectra and the identification of the fundamental resonance frequency. However, instead of calculating the H/V from amplitude spectra, as suggested by Zhu et al. (2020), we demonstrate how we obtain stable H/V spectral ratios by first calculating Power Spectral Density (PSD) curves (McNamara and Buland, 2004) from the recorded data before we make the H/V division.

H/V spectral ratios can be calculated from seismic events, teleseismic phases or from the ambient seismic noise field. Due to almost four years of deployment of the Groningen network, abundant ambient noise data and teleseismic event recordings are available and are used as a tool for estimating shear-wave velocities. In Groningen, the ambient noise field contains a frequency- and time-dependent mixture of body and surface waves. This makes it doubtful whether the computed H/V ratios need to be interpreted in terms of surface-wave ellipticities (Malischewsky and Scherbaum, 2004), body-wave resonances (Nakamura, 1989, 2019) or a mixture of wave types (Sánchez-Sesma et al., 2011; Lunedei and Malischewsky, 2015; Spica et al., 2018a). For that reason, we start off with using teleseismic body-wave phases, for which the interpretation in terms of

body-wave resonances is straightforward. Subsequently, we compute H/V ratios from the ambient noise field and compare it with modelling and the pure body-wave results to obtain more insights in the composition of the noise field.

In this paper, we apply the H/V methodology to estimate average shear-wave velocities of the soft Cenozoic sedimentary cover in Groningen, called the North Sea Group (NSG). The current velocity model by Kruiver et al. (2017) is an accurate field-scale description for the upper 120m of the soft sedimentary layer, but the shear-wave velocities in the lower part of the NSG are based on single V_p/V_s ratios derived from only 2 well logs, causing large uncertainties in the lateral variation of the velocities in this part of the sedimentary cover, stretching to about 800m depth. Detailed shear-wave velocities are known at all borehole seismic stations, but only for the upper 200 m (Hofman et al., 2017). We aim to update the shear-wave velocities for the sedimentary cover below 200m (Lower NSG) at each borehole station, to act as input velocity model for hypocentre localisation of the seismic events at the 200 m deep seismometer in each of the 70 stations of the Groningen borehole network (Dost et al., 2017). The depth of the base North Sea Group is based on lithostratigraphy of hundreds of production wells in the Groningen gas field (Van Dalfsen et al., 2006). Therefore this depth is a very reliable parameter to base the calculations of the shear wave velocities on. The shear-wave velocity model from Kruiver et al. (2017) acts as reference model to compare our model with.

2 Geological Setting

The area of interest is the northeast of the province of Groningen, with a flat topography, close to mean sea-level and a water table almost up to the surface. The sedimentary cover of interest is formed by the Cenozoic soft sediments, named the North Sea Group (NSG), including the Upper, Middle and Lower North Sea Groups (Fig. 1) (Mulders, 2003; Vos, 2015). The top of the underlying Upper Cretaceous limestones (Chalk Group) is defined as reference horizon in previous site response studies (Rodriguez-Marek et al., 2017) and recent hazard models (Bommer et al., 2017; Kruiver et al., 2017).

The North Sea Group has an average thicknesses of about 800m, with local variations in depth due to underlying salt diapirs and basin deepening towards the north. Paleogene and Neogene sediments mostly consist of transgressive marine clays alternated with continental siliciclastic sediments. At around 500-600m depth, a high velocity layer (Brussel Sand Member) of compacted sands is deposited during a phase of regression and subsequently partly eroded. Marine delta slope deposits consisting of clays and sands are dominating the upper part of the North Sea Group, unconformibly overlain by Quaternary glacial deposits (Wong et al., 2007). The Pleistocene sedimentary sequence is characterized by fluvial, eolian, glacial and marine deposits, that are crosscut by deep (down to 200m) glacial tunnel valleys which are filled with sand and compacted clays, named the Peelo formation. Very soft Holocene tidal channel sands, marine clays and peat form the upper 10-20m of the Groningen subsurface (Meijles, 2015; Wong et al., 2007).

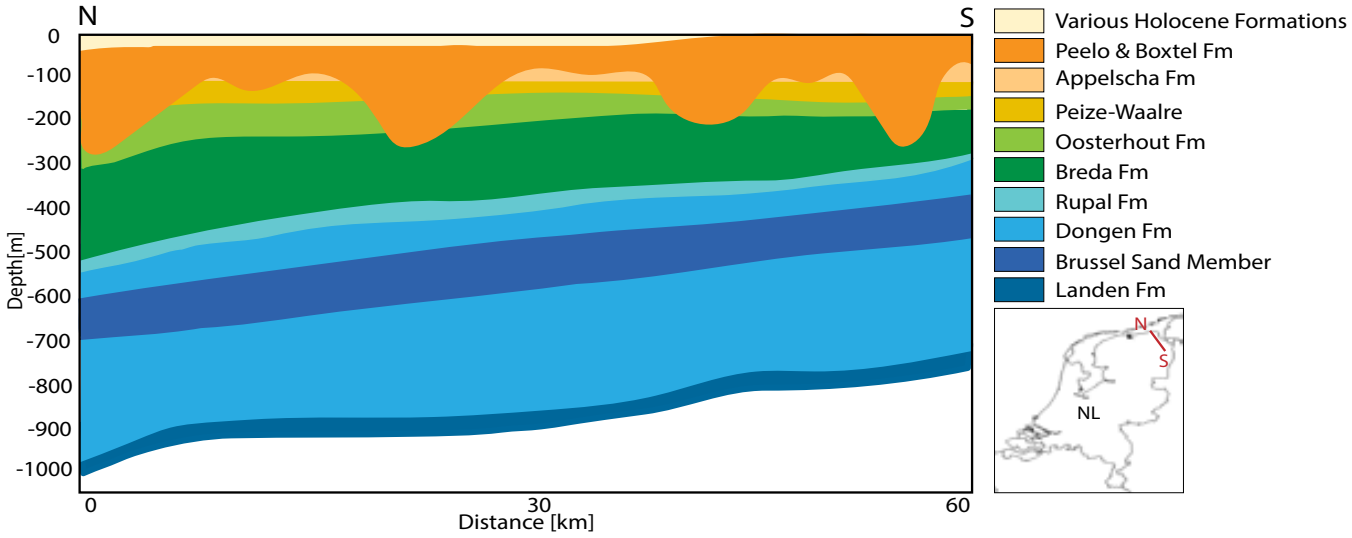

Figure 1. Schematic cross section of the North Sea Group (NSG) based on formation depths from www.dinoloket.nl and stratigraphic charts (Wong et al., 2007). The formations of the Lower NSG have blue colours, formations of the Middle NSG are in Green and Quaternary formations of the Upper NSG are in orange/yellow . From the different Members in the lower NSG, only the Brussel Sand is included due to its importance for this study.

3 Existing velocity models

Kruiver et al. (2017) have built an integrated shear-wave velocity model for the Groningen area from the surface to the base of NSG. In this 3-D velocity model, large amounts of geological, geotechnical and geophysical observations are merged. Due to the rich data availability for the upper 40m, the model is very detailed in this depth range (Noorlandt et al., 2018). At depths of 40-120m, less detail is available as the velocity model model is constrained through inversion of surface waves (recorded as noise) from reflection seismic surveys. shear-wave velocities in the deepest part are derived from a pre-existing pressure-wave velocity model from reflection seismics and the conversion ratio is based on two borehole sonic logs (Zeerijp and Borgsweer). We refer to this velocity model as the Deltares-NAM model. Mainly for the deeper section of the NSG, the uncertainties are high for the shear-wave velocities since they are derived from a single V_p/V_s ratio. Pressure-wave velocities show lateral heterogeneity. A conversion to shear-wave velocities away from the wells where the V_p/V_s ratios were determined, leads to errors. For accurate localisation of the earthquakes, a shear-wave velocity profile for the lower NSG for each station site is required.

Hofman et al. (2017) derived vertical seismic velocity profiles for both P- and S waves for nearly all stations in the Groningen network, using seismic interferometry applied to local event data. Their method estimated velocities within four intervals from 0m to 200m depth. These velocity models are in general in good agreement with the Deltares-NAM and model, as is shown in Noorlandt et al. (2018). Our study benefits from this detailed shallow velocity structure, which we use, at the seismic stations,

for the upper 200m of the North Sea Group.

Spica et al. (2017) presented a comparison between the model from Kruiver et al. (2017) and velocities derived from the H/V spectral ratio for the upper 200m from 10 stations in the Groningen network. Inversion of the H/V spectral ratios based on the diffuse field assumption (Sánchez-Sesma et al., 2011) are developed to gather constraints on the shear-wave velocities. Subsequently, Spica et al. (2018b) assessed the velocity structure at 415 sites for a temporarily deployed dense surface array, covering only a small part of the Groningen gas field, through joint inversion of multimode Love-and Rayleigh wave dispersion curves and H/V spectral ratios. From this similar dense array, Chmiel et al. (2019) obtained shear-wave velocity models by using depth inversions of surface waves from ambient noise. They were able to derive velocities up to base NSG by adding depth constraints to overcome weak sensitivities of surface waves at these depths.

Although several high quality shear-wave velocity profiles across different scales became available over the last years, in situ velocity measurements for each seismic station in the Groningen network are missing and form the objective of our work.

4 Data set

To conduct the present study, the KNMI shallow borehole network (further referred to as G-network) was chosen, which has both borehole and surface seismographs. The G-network installed on top of the Groningen gasfield consists of 69 stations (Dost et al., 2017) and Fig. 2 shows the distribution of the seismic stations in Groningen. Each station is equipped with three-component, 4.5 Hz seismometers at 50m depth intervals (50, 100, 150, 200 m) and an accelerometer at the surface. The stations are continuously recording since 2015 and the data is available via the data portal of Royal Netherlands Meteorological Institute (KNMI, 1993). We use a large three-component data set of ambient noise and five strong teleseimic events (Table 1) measured by the G-network. Several strong teleseismic events are required to obtain an estimate of the H/V ratios and the standard deviation thereof. We refer to 'station' for the entire string with 1 accelerometer and 4 geophones, and refer to 'seismometer' for a single sensor measurement at a certain depth. For calibration purposes we use one broadband seismometer which is nearly co-located with one of the geophones.

Table 1. List of teleseismic events used for this study

Event	Magnitude	Origin date	Origin time (UTC)	Wave phase
Mexico (Chiapas)	8.1	September 8, 2017	04:49:21	S
Alaska (Kodiak)	7.9	January 23, 2018	09:31:42	S
Venezuela (Sucre)	7.3	August 21, 2018	21:31:44	S
Peru	8.0	March 01, 2019	08:50:44	S
Southern California	7.1	July 6, 2019	03:19:58	S

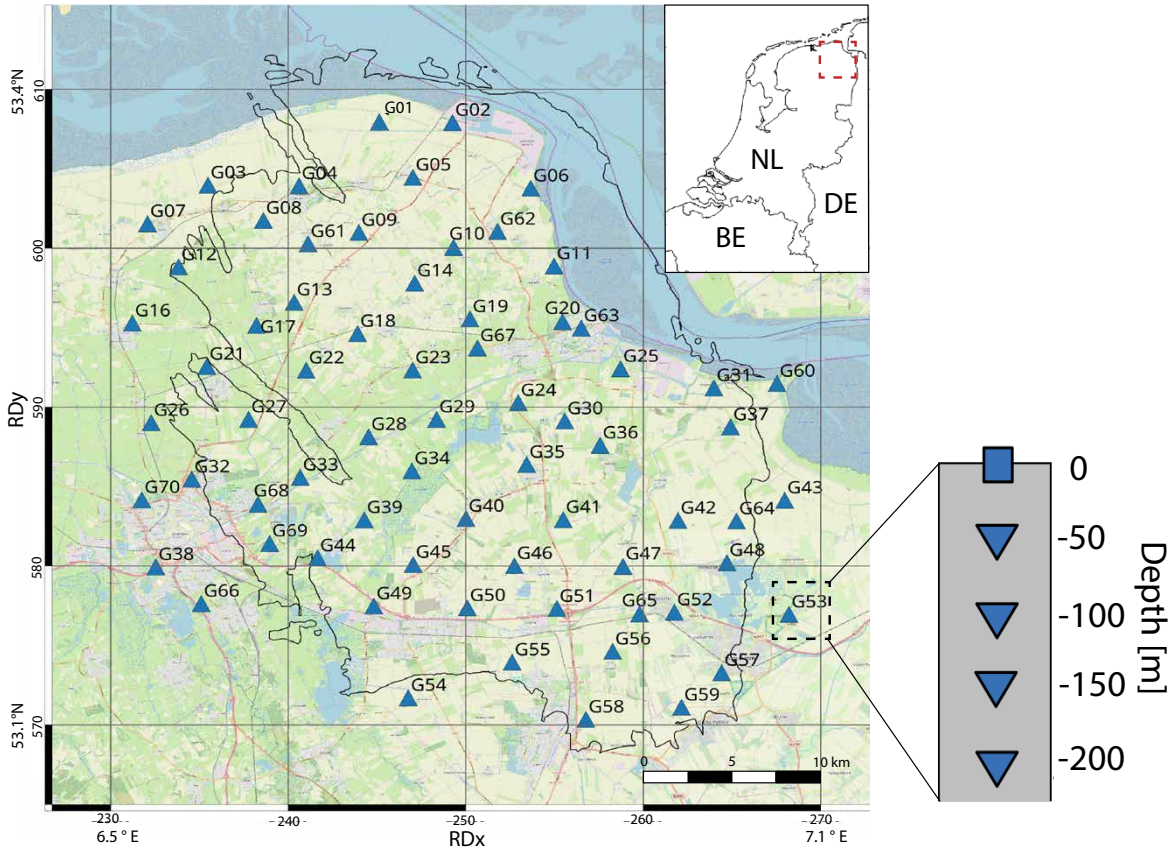

Figure 2. Map view of the Groningen area. The triangles represent the surface location of the stations of the G-network. Each station contains an accelerometer at the surface (square) and 4 geophones at 50 depth intervals (inverted triangles). Coordinates are shown within the Dutch National Triangulation Grid (Rijksdriehoekstelsel or RD) and lat/lon coordinates in the corners for international referencing. Background map: © OpenStreetMap contributors, CC-BY-SA, www.openstreetmap.org.

5 Velocity Profiles from teleseismic phases

Multiple strong (M>7.0) global teleseismic phases are recorded within the G-network. With their arrivals, body waves resonate between the free surface and the large impedance contrast between the soft sediment layer and the seismic bedrock, resulting in both vertical and horizontal motions. Teleseismic S-phases are transmitted into the NSG with angles smaller than 5 degrees with vertical. The size of the underlying impedance contrast determines how strongly the waves are reflected and thus how much of the wave energy is trapped. The interference of multiple reverberations within the soft layer leads to a resonance pattern in which certain frequencies are amplified and others interfere destructively.

From five teleseismic arrivals, 1000 s time windows are taken, starting just prior the S-phase onset. The direct S phase, the later coda and the subsequent weaker shear-wave phases are included in this window. Figure 3 shows a seismogram for the Mexico M8.1 event for a soft-sedimentary site in Groningen and a hard-rock site in the south of the Netherlands. Both stations have a comparable distance to the event (9359 vs 9378 km). A time window around the P-phase and S-phase is shown. Their amplitude is larger at (a) than at (b) mainly due to amplification over the soft sediments. Also, the basin setting for (a) leads to stronger coda. The response is band-pass filtered between 0.03 and 2 Hz. This is a low frequency band for the equipped geophones and accelerometers. The lower part of this band, from 0.03 to about 0.2 Hz, is indeed most of the time dominated by instrumental noise. Strong teleseismic arrivals, however, are still well recorded down to 0.03 Hz. Their amplitudes are up till a factor 1000 higher than the microseism. Events with magnitudes above 7.0 and with distances up till 90 degrees, produce S-phases with sufficient energy to compute H/V curves that contain resonances of the entire sedimentary sequence.

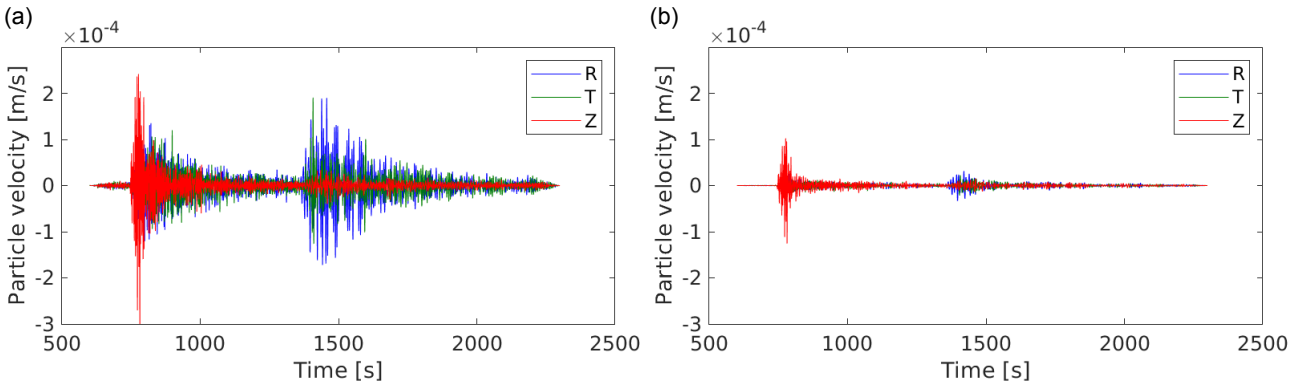

Figure 3. Comparison of the Mexico M8.1 event (Table 1) recorded on (a) a soft-sediment site in Groningen (seismometer G300) and (b) at a hard-rock site (seismometer HGN) in the south of the Netherlands. R=radial, T=transverse, Z=vertical component of the seismometer.

5.1 Identification of resonance frequencies using teleseismic phases

Conventional H/V curves are computed based on Fourier amplitude spectra (FAS) (e.g. in Bard (2002), or with response spectra (Zhu et al., 2020). Here we present how we calculate H/V curves from power spectrum densities (PSDs). Computation of a PSD starts with computing a FAS, which is the absolute value of the discrete Fourier transform: $|F|$. Computing the PSD amounts to

$$PSD = 2|F|^2 \frac{\Delta t^2}{T^2}, \tag{1}$$

where Δt is the sample duration and T the duration of the time window that was used to compute the FAS. The factor of two only needs to be applied when merely positive frequencies are used. The PSD is a frequency-normalized version of the power spectrum, which normalization makes the spectrum less sensitive to input data duration T (Havskov and Alguacil, 2004). Our

main reason to start of with PSDs instead of FAS is that PSDs are already routinely computed for data inspection and quality checking purposes (McNamara and Buland, 2004). In the computation of PSDs, we follow the recipe of (Peterson, 1993) which results in well-averaged spectra, which is elementary for usage in H/V computation. A large difference with typical PSD computations is that we do not apply any smoothing.

From a 1000s window, containing the P-and S-phase of the teleseimic arrival, PSDs are computed using time windows of 102.4s with a 75% overlap (Peterson, 1993). The two horizontal components are averaged by vector summation and subsequently the horizontal-to-vertical ratio is taken from the PSDs, resulting in the body wave H/V ratio (HVBW):

$$HVBW = \frac{\sqrt{PSD_E + PSD_N}}{\sqrt{PSD_Z}}, \tag{2}$$

where the subscripts $_E$, $_N$ and $_Z$ denote the east, north and vertical component, respectively. When substituting Eq. 1 into the above equation, one finds that the PSD-based HVWB is consistent with a FAS-based H/V computation:

$$HVBW = \frac{\sqrt{|F_E|^2 + |F_N|^2}}{|F_Z|}, \tag{3}$$

in which the FAS of both horizontal components is combined through vector summation. No smoothing is applied since smoothing will affect the picking of the exact fundamental resonance peak. For sites with multiple significant peaks, smoothing could result in a shift to higher frequencies and a bias in identification of the fundamental resonance peak (Zhu et al., 2020). Albarello and Lunedei (2013) present several alternative procedures to average the horizontal components for computing ambient noise H/V ratios, and conclude that vector summation is the most physically logic averaging method, therefore this averaging procedure has been applied on the two horizontal-component PSDs. Nevertheless we tested the different methods and found no difference in resulting peak frequencies for our dataset, but biases may arise between the different averaging methods when evaluating the amplitude of the H/V peak (Albarello and Lunedei, 2013).

All borehole seismometers measure the same fundamental resonance (f_0) of the entire soft-sedimentary column. This is shown in Fig. 4 for the Deltares-NAM model at station G24. The amplitude of $f_0 = 0.18$ Hz, does vary over the different depth levels. The instruments at depth experience notches due to interference of up-and down-going waves. For larger depths, the notches shift to lower frequencies; in Fig. 4 the first notch for the 200m depth instrument can be identified at 0.55 Hz. The interference of the notch with f_0 leads also to a shift in frequency. Since the frequency perturbation is less than 0.01 Hz, it is decided to calculate the mean HVBW over all depth levels to better cancel out noise and to obtain a more stable result for picking f_0.

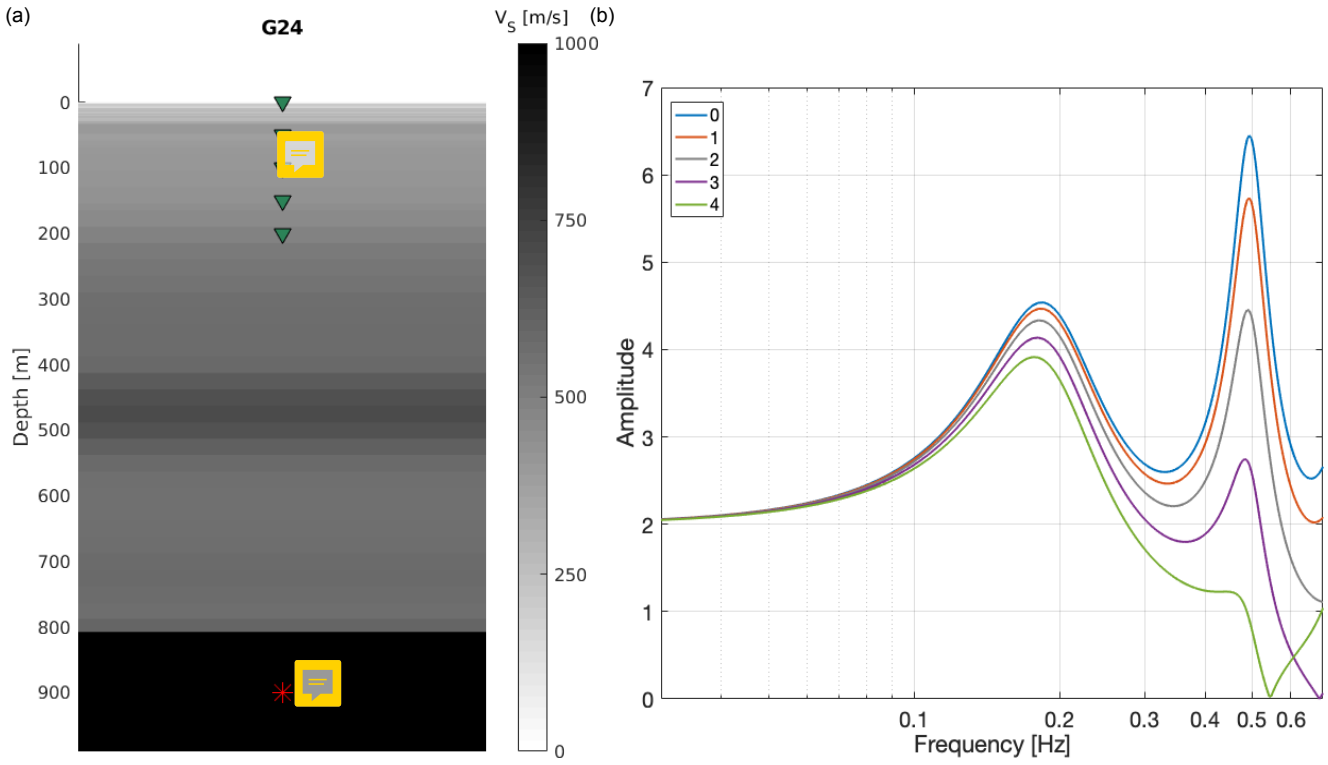

Figure 4. (a) velocity profile from the Deltares-NAM model at station G24. The top 800 m is made up of the NSG with much lower V_S than the underlying Chalk Group. The green triangles denote instrumented depth levels. (b) forward modelled amplitude spectra (coloured lines) for a vertically incident shear wave, recorded at the 5 different depth levels. Both the fundamental mode and first higher mode of the entire sedimentary column can be seen. Also, waves resonate between the free surface and the high velocity layer at 450m depth (Brussels Sands). The resulting fundamental mode interferes with the first higher mode of the entire NSG and results in the elevated peak just below 0.5 Hz.

We compute the HVBWs (Eq. 2) for five teleseismic arrivals (Table 1) and Fig. 5 shows example HVBW curves for station G24. Note that, though the amplitudes are slightly different, the frequency of the main peak (f_0) is consistent from event to event. Frequencies above 0.7 Hz are omitted since the S-phase provides insufficient energy above this frequency threshold.

By applying the H/V method on teleseismic phases, the source and path effect are largely suppressed to focus on the site effect. However, this suppression is always incomplete. Furthermore, we assume vertical incidence but in reality this is not obtained. These two facts explain the difference in amplitudes of the resonance peak for each event, despite the uniform subsurface. Some HVBW curves show multiple peaks near the f_0 (Fig. 5a,d), causing a challenge to distinguish the peak corresponding to the resonance of the entire North Sea Group. Comparing HVBW curves from different events helps to pick the peak belonging to the fundamental resonance frequency and by averaging over multiple events, the error in the mean f_0 is minimized.

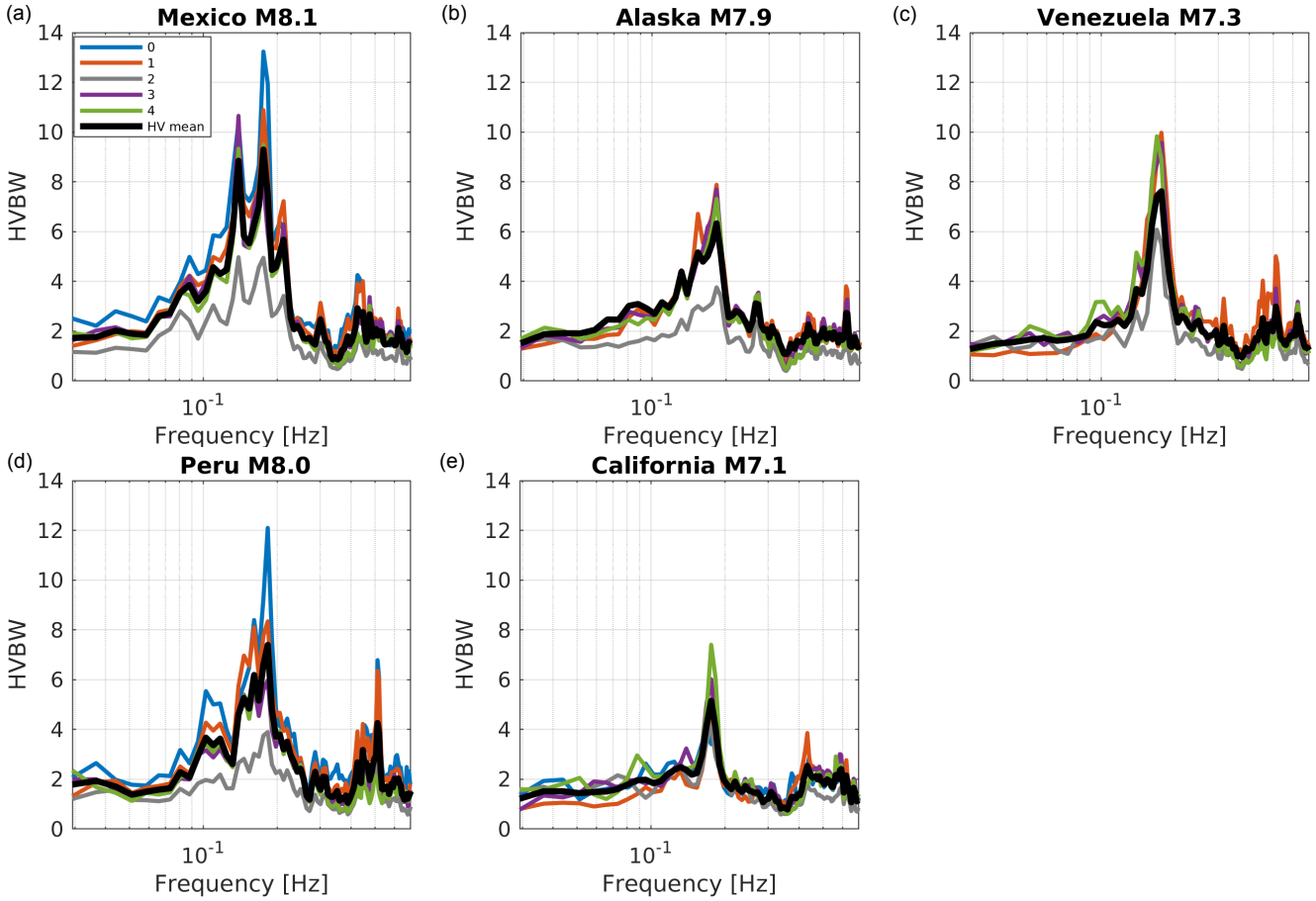

Figure 5. Horizontal-to-vertical spectral ratios from body wave arrivals (HVBW) from five teleseismic events for station G24. The black line is the calculated mean HVBW over five HVBWs (coloured lines) corresponding to five seismometers per station. The peak frequency of the HVBW (f_0) is picked for shear wave velocity calculations using Eq. 4. (a) Mexico M8.1 (b) Alaska M7.9 (c) Venezuela M7.3 (d) Peru M8.0 (e) Southern California M7.1

5.2 Calculating shear-wave velocities

190 From the HVBW we interpret the prominent low-frequency peak as the fundamental shear-wave resonance frequency (f_0) of the complete NSG package. From each HVBW peak (f_0) and the well established depth of the base of the unconsolidated sedimentary layer (NSG) (Van Dalfsen et al., 2006), shear-wave velocities can be calculated based on (Tsai, 1970), assuming vertical incident body-wave contribution:

$$f_0 = \frac{V_s}{4d}, \tag{4}$$

where f_0 represents the fundamental resonance frequency, V_s is the (harmonically averaged) shear-wave velocity from surface to the bed rock interface, and d the depth of the base of the NSG. Since the depth of the NSG is accurately defined from 3D reflection seismics in combination with lithostratigraphic marks of hundreds of boreholes (Van Dalfsen et al., 2006; Kruiver et al., 2017), the shear-wave velocity is straightforwardly calculated. Per station and for each teleseismic event, the velocity is calculated with Eq. 4, and subsequently the five shear-wave velocities are averaged. This averaged shear-wave velocity for each station is referred to as V_s^{NSG} and is plotted in Fig. 6a. Stations G45 and G52 are discarded, due to the scattering effect of the underlying salt domes, the local 1D assumption is here not valid to calculate velocities using Eq. 4. After all, for 63 stations shear-wave velocities are calculated.

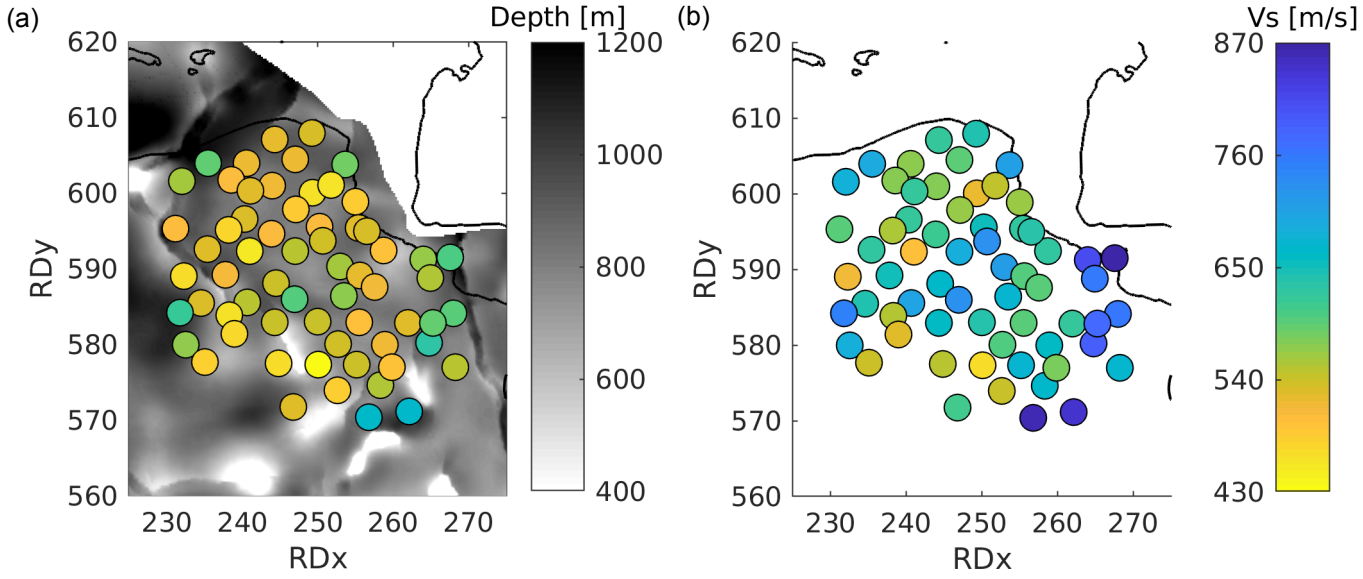

Figure 6. Average shear-wave velocities for the North Sea Group from each station in the Groningen network. Coordinates are plotted in Rijksdriehoek (RD) projection. (a) Map of the depth of base North Sea Group (Van Dalfsen et al., 2006) with, in circles, the average shear wave velocities for the entire North Sea Group (V_s^{NSG}). (b) Average shear-wave velocities calculated according to Eq. 5 for the lower part of the NSG (V_s^{NSL}): from 200m depth till the base of the sedimentary cover.

Hofman et al. (2017) have constructed detailed shear-wave velocity profiles of the upper 200m at G-network stations (V_s^{200}). The teleseismic velocity profiles (V_s^{NSG}) give velocities for the complete NSG. Per station, an estimate of the average S-wave velocity of the lower NSG (V_s^{NSL}) is obtained by combining the V_s^{NSG} and V_s^{200} estimates using

$$\frac{z^{NSL}}{V_s^{NSL}} = \frac{z^{NSG}}{V_s^{NSG}} - \frac{z^{200}}{V_s^{200}}, \tag{5}$$

which corresponds to harmonic de-averaging. This calculation is done for each station (Fig. 6b), where z^{NSG} represents the thickness of the entire NSG and z^{NSL} the thickness of the lower part of the NSG. Fig. 7 shows four examples of velocity profiles constructed with this method. For each station, these profiles are used as input for forward modelling (Section 7).

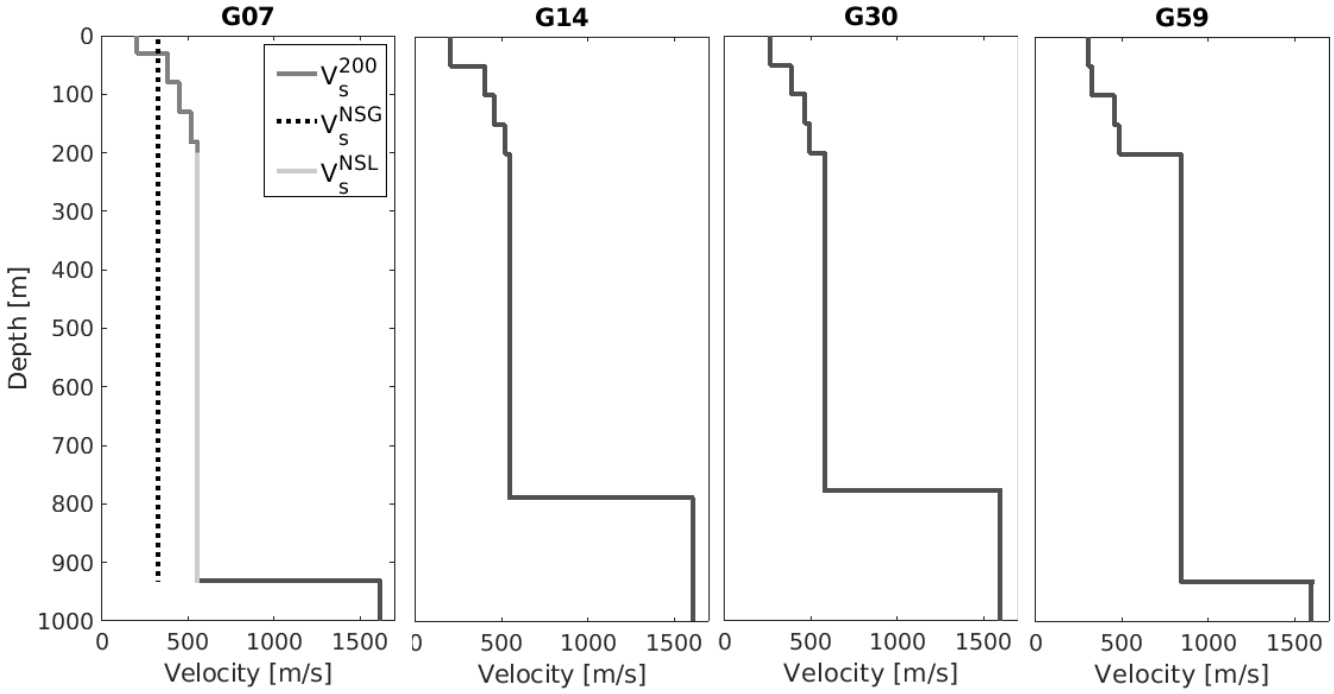

Figure 7. Subsurface velocity profiles from resp. station G07, G14, G30 and G59. The panel on the left shows the construction of a merged S wave profile: velocity profiles of the upper 200m (Vs200, dark grey line) are taken from Hofman et al. (2017), the entire NSG average velocity (V_s^{NSG}, dotted line) from teleseismic phases. The V_s^{NSL} (light grey line) is calculated from the V_s^{200} and V_s^{NSG} (Eq. 5). The velocity contrast at around 800m depth is between the base NSG and top Chalk Group.

For all stations, the standard deviation of the average V_s^{NSG} over five teleseismic events is calculated and plotted in Fig. This Figure shows the variation of the estimated velocity over the 63 sites. If we leave out the outliers G58 and G59, we get an average shear-wave velocity and standard deviation of V_s^{NSG} over Groningen of 526 m/s and 31 m/s, respectively. For V_s^{NSL} the average velocity and the standard deviation are 637 m/s and 59 m/s, respectively. Higher standard deviations for the V_s^{NSL} can be explained by the same error being attributed to only the lower NSG instead of the entire NSG.

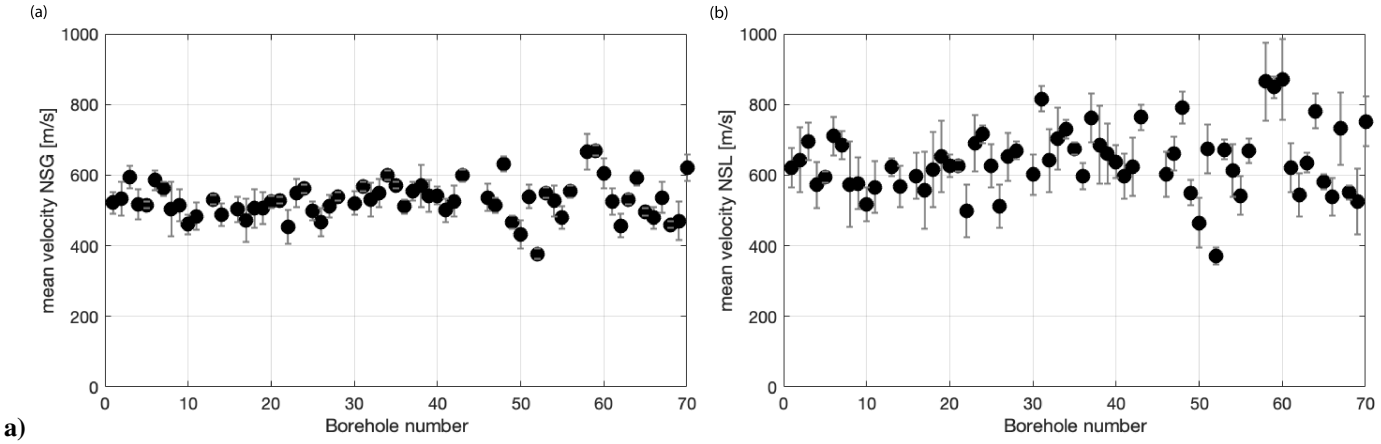

Figure 8. Average shear wave velocities (black dots) and standard deviation (grey bars) derived from the H/V ratio of five teleseismic events, sorted on station number for (a) the V_s^{NSG} and (b) the V_s^{NSL}.

5.3 Calculating an empirical bedrock-depth function

In the previous section we took advantage of the well constrained depth of the unconsolidated sediments to invert for S-wave velocity. In other areas in the Netherlands, similar sedimentary fills exist, but the depth of the NSG is less well constrained. Some areas might do have constraints from a few deep wells, but many les than in Groningen. Other areas rely on reflection seismic data and again other areas have neither of the two. For these regions outside Groningen, one could either use equation 4 together with an average NSG shear-wave velocity as found in the previous section. Alternatively, one could find an empirical relation connecting depth d with resonance frequency f_0 in the form

$$d = a f_0^b, \tag{6}$$

as introduced by Ibs-von Seht and Wohlenberg (1999). Comparing Eqs. 4 and 6 one can see that if the lossless single-resonating wave assumption is taken (Eq. 4) the factor a and b in Eq. 6 correspond to $V_s/4$ and -1, respectively.

Fig. 9 shows the f_0-depth distribution and least-squares fit of Eq. 6, yielding as a mean model for the NSG sediments:

$$d = 206 f_0^{-0.755}. \tag{7}$$

and a depth standard deviation of 73 m. Using the mean depth of the dataset (814 m), this corresponds to a standard deviation of 9 %. In comparison, the model that Ibs-von Seht and Wohlenberg (1999) found in the Aachen area (Germany) is shown. Clearly, using the latter model would yield a too deep sedimentary fill for the Netherlands. Here we show that the sedimentary setting in the Netherlands is different to fitted models around the world, as summarized in Thabet (2019), leading to different values for a and b. The marine and clay-rich sediments of the NSG are of very young age, therefore no less compaction has strengthened the material.

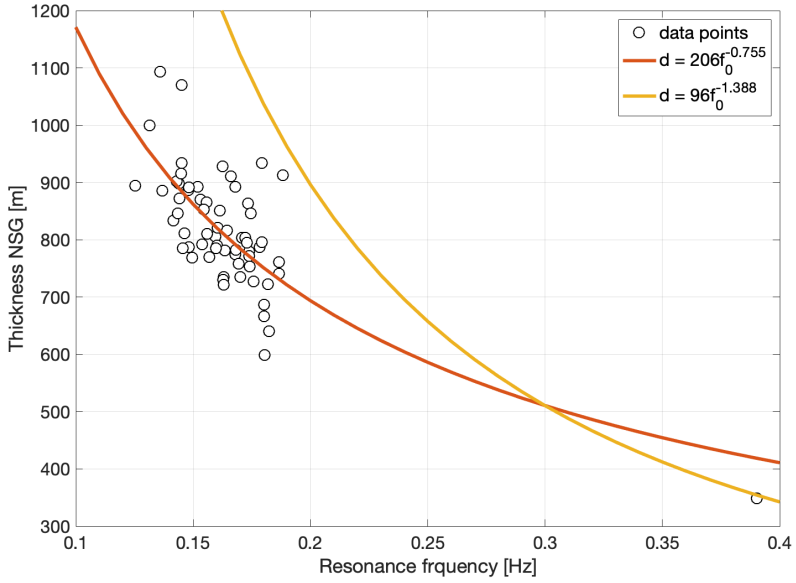

Figure 9. The thickness of NSG versus fundamental resonance frequency f_0 distribution for 63 sites in Groningen (black circles), together with the least-squares fitted function (orange line) and the empirical model for the Aachen region (yellow line) as obtained by Ibs-von Seht and Wohlenberg (1999).

6 Probability density functions of ambient noise H/V spectral ratios

In the previous section, we presented site specific shear-wave velocities based on the fundamental resonance frequency from teleseismic phases. The majority of studies on H/V spectral ratios are based on recordings of the ambient noise field. Therefore in this section, we calculate the H/V from the ambient noise field and performed forward modeling including the velocity profiles established in Section 5. This enables us to quality check the H/V method applied on teleseismic arrivals. Multiple years of ambient noise recordings are available and to obtain stable H/V ratios we employ a sequence of averaging procedures as outlined below.

Similar to the teleseismic recordings, power spectral densities (PSDs) are calculated from ambient noise data for all 3 components for the 50 m depth seismometers in the Groningen network. One-day ambient-noise records are divided into time windows and for each time frame the PSD (Eq. 1) is calculated, using 75 % overlapping time segments. Each segment is 2^{14} time samples (82 seconds) long. Subsequently, for each day, an H/V ratio is computed from the PSDs by implementing Eq.2. In McNamara and Buland (2004) the probability density function (PDF) of the PSD is computed. This allows separating long-term noise conditions from transient events and time periods with sensor malfunctioning. We follow a similar approach as McNamara and Buland (2004), but instead of a PDF of the PSD, we compute a PDF of the ambient-noise H/V ratios. This

distribution we further refer to as PDF HVAN. Figure 10 shows examples. In a conventional H/V plot, there would be a mean H/V value for each frequency, or a mean value and a confidence zone, based on a normally distributed error model. Instead, the PDF shows the complete digitized H/V probability distribution for each frequency. From this distribution, the mean, mode, median and different percentiles, can be taken.

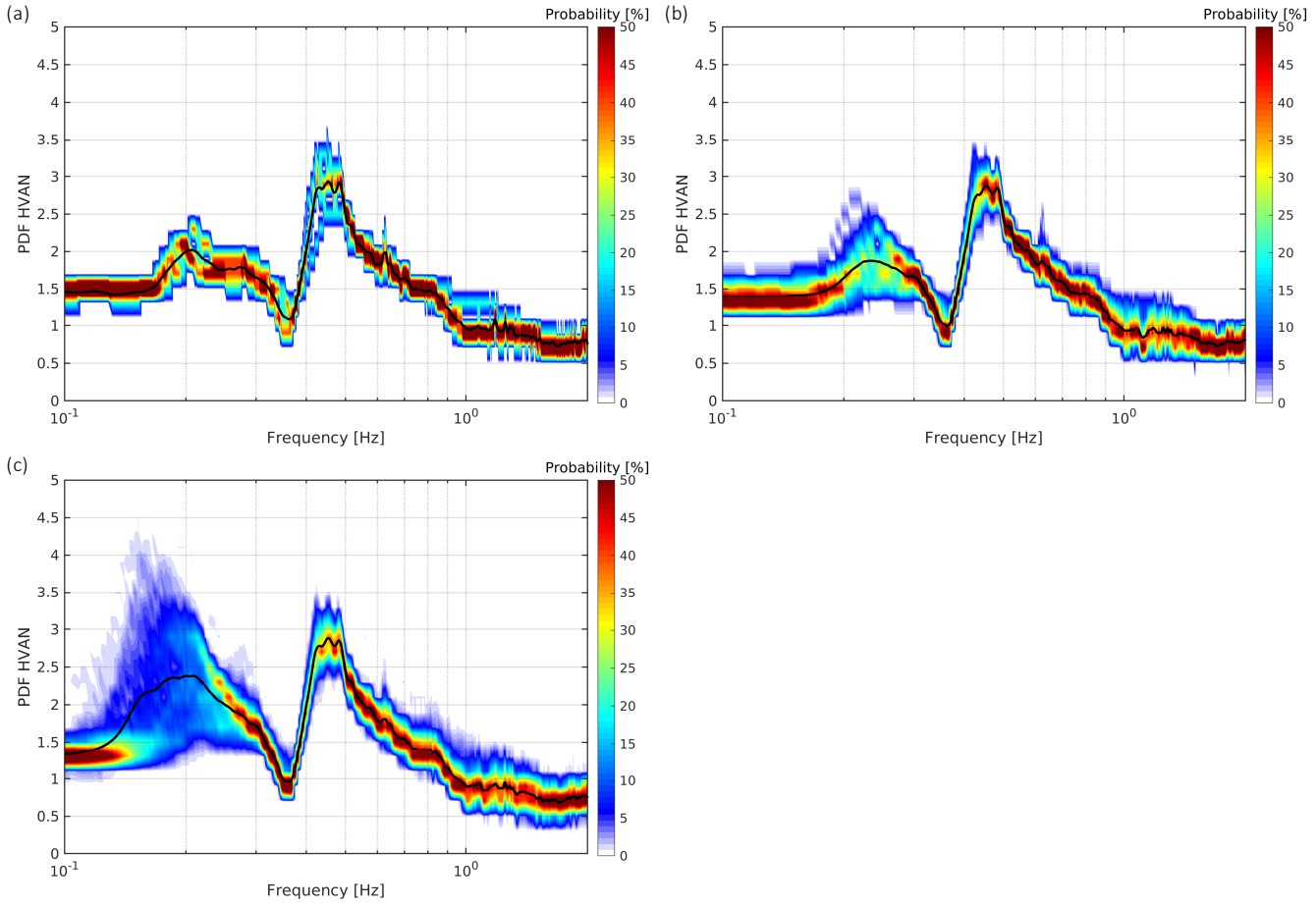

Figure 10. Probability density functions (PDF) from ambient noise horizontal- to-vertical spectral ratios (HVAN) for station G39, 50m level. The black line represents the mean. (a) PDF HVAN for one week (21/03/2017-28/03/2017). (b) PDF HVAN for one month (01/05/2017-01/06/2017). (c) PDF HVAN for one year (01/02/2017-01/02/2018).

Generally, H/V calculations are based on noise measurements of largely varying duration: for less than 1 hour e.g.(Fäh et al., 2001; Scherbaum et al., 2003), a few days (Ruigrok et al., 2012) or up to a month (Parolai et al., 2002). Due to the permanent deployment of the network in Groningen, noise has been recorded for almost three years. This creates an excellent opportunity to test what minimum window of noise data yields a stable H/V curve. Furthermore, by measuring a long period of noise, the HVAN can be expressed as a PDF for any desired period for each seismometer in the network. Figure 10 shows distribution

plots of respectively one week, one month and one year of the calculated PDF HVAN. A stable peak around 0.4 Hz is created by at least one month of recording of the ambient noise field. This one month is the preferred duration because of manageable data handling instead of a year of data. Therefore, for all stations at 50 m depth, one month of ambient noise data is used to compute the PDF HVAN. From this distribution, the mean H/V ratio (which we further refer to as HVAN) is extracted. This HVAN is likely descriptive of the site, rather than a remnant of source or path effects.

For the 4.5 Hz seismometers in the G-network, instrument noise is dominating frequencies below 0.2 Hz, where also the fundamental mode of the NSG resonance is expected. Due to large storms across the year, in which the microseism noise surpasses the instrumental noise, the computed PDF HVAN for one year (Fig. 10c) shows a peak around the fundamental resonance frequency (0.15 Hz) of the NSG. In case of an energetic ocean state, the amplitudes in the fundamental mode are similar to the higher mode peak. However, over the year the probability is low and picking the corresponding peak frequency is unreliable. In August 2018, 4 broadband seismometers were installed in Groningen at 100m depth. With this broadband data we are able to confirm the recordings of the fundamental mode of the NSG. Figure 11a) shows the PDF HVAN for broadband station G82B which does have a clearly resolved peak for the fundamental frequency. Due to the unreliability of the fundamental mode peak in the G-network geophones and accelerometers, in the following we focus on the subsequent notch, between 0.3 and 0.4 Hz (Fig. 10).

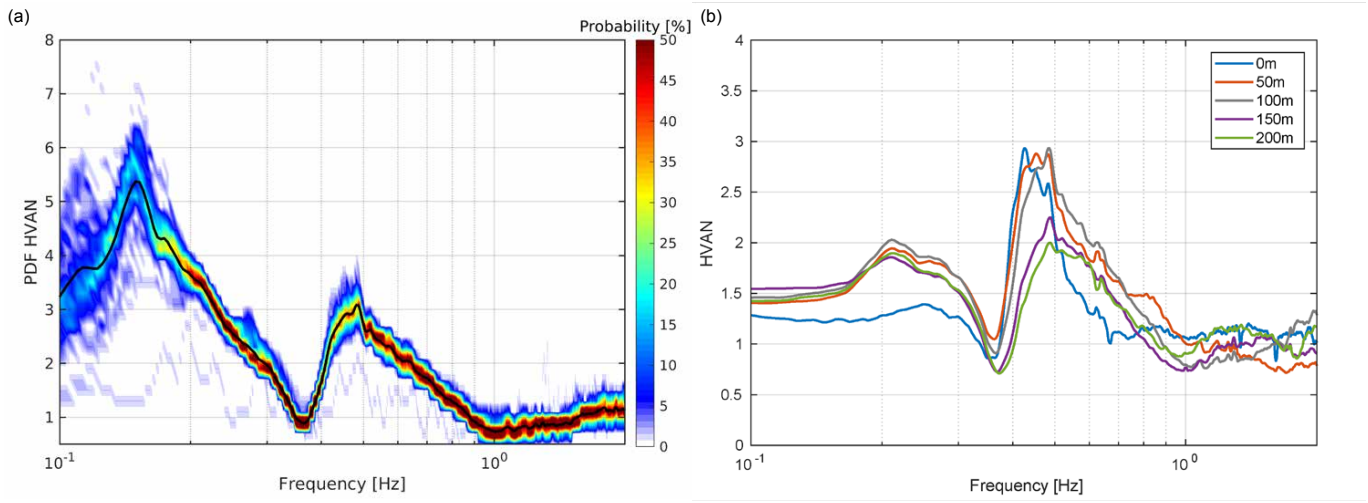

Figure 11. (a) PDF HVAN for one month (01/09/2018-01/10/2018) at broadband station G82B, located within 100 m of G39, and has a depth of 100m. The broadband PDF HVAN displays a peak for the fundamental mode (around 0.15Hz) and the secondary peak (around 0.45Hz) reflects the higher mode for Rayleigh waves. The black line indicates the mean from the PDF HVAN. (b) HVAN curves for one month for station G39 for all depth levels.

Triggered by a study by Lontsi et al. (2015), the depth dependency of the H/V curve across a downhole array is evaluated in Fig. 11b. With increasing seismometer depth, a maximum shift (0.06 Hz) of the higher-mode peak is observed. For the surface

accelerometer, nearly all ground motion falls outside its dynamic range, below 0.3 Hz. The instrumental noise has the same level on all 3 components. As a consequence, the H/V ratio is close to 1 below 0.3 Hz, whereas the geophones still have a small sensitivity down to 0.2 Hz. The remaining pattern of the H/V curves in Fig. 11 are consistent with Fig. 3b, were the body-wave H/V amplitude is decreasing as function of depth. Here, we use the seismometer at 50 meter depth, where anthropogenic noise is considerably less than at the Earth's surface and hence a more stable HVAN can be computed. The software (Geopsy) used for forward modeling assumes measurements at the surface, therefore the 50 m depth station is preferred over the deeper levels.

7 Surface- and body wave forward modeling

Commonly, the ambient seismic field is dominated by surface waves (Aki and Richards, 2002; Bonnefoy-Claudet et al., 2006a, b). Ocean-generated seismic noise (microseism) is measured on the Groningen seismometers from 0.1-1.0 Hz. Here, the low-frequency ambient seismic field is composed of microseisms induced by Atlantic-Ocean gravity waves, while the higher frequencies are mainly induced by North-Sea gravity waves. Both sources have a main propagation direction from the northwest (Spica et al., 2018a; Kimman et al., 2012). Spica et al. (2018b) discuss the wave field in Groningen up to 0.6 Hz and conclude that the H/V peak around 0.15 Hz is dominated by Rayleigh waves and the H/V peak around 0.4 Hz by body waves. Moreover, a review of Lunedei and Malischewsky (2015) expresses the view that H/V curves are composed by the whole ambient-vibration wave field, although not in equally distributed proportions. To better understand the measured H/V curves and to create a perspective on the composition of the microseismic ambient noise field, we perform both body-wave forward modeling (shear wave resonance) and surface-wave forward modeling (Rayleigh-wave ellipticity).

7.1 Body-wave forward modeling

Body-wave forward modeling is performed using OpenHVSR, developed by Bignardi et al. (2016). This software computes theoretical transfer functions of layered soil models based on the fast recursive algorithm from Tsai (1970). For the forward model input files we use the subsurface shear-wave velocity profiles as described in Section 5. To the 5-layer over a halfspace velocity models, we add also a 5-layer seismic quality factor. Q-values of resp. 10, 50, 50, 50 and 100 are determined from the borehole stations. Pressure-wave velocities are derived from existing velocity models (Van Dalfsen et al., 2006). The body-wave forward model (Fig. 12) shows modeled shear- and pressure-wave resonance spectra and is combined with the HVAN curve and the HVBW from station G39. The fundamental frequency for the HVBW has quite a good fit with the modeled body-wave resonance.

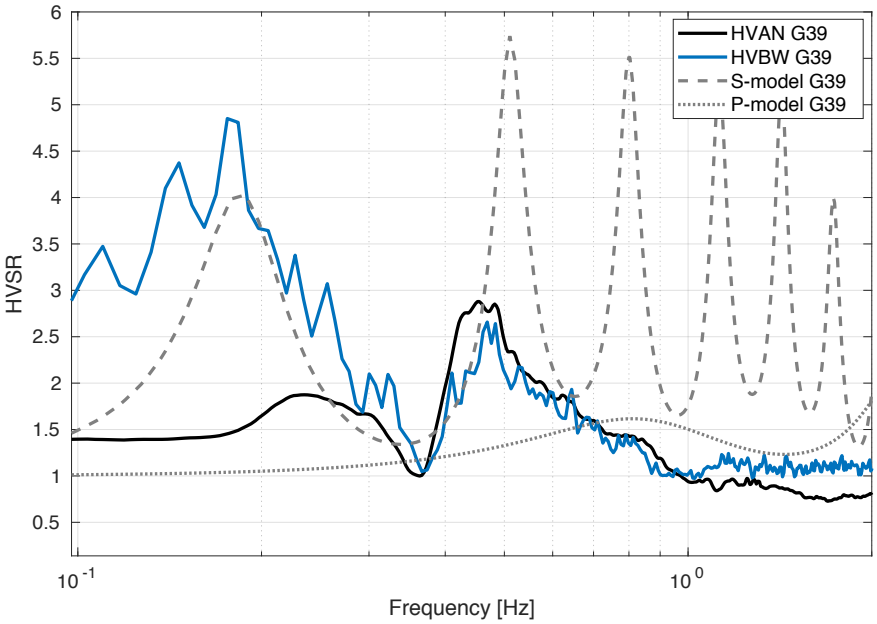

Figure 12. Modeled shear wave resonance (dashed line), pressure wave resonance (dotted line), HVAN (black solid line) and the HVBW (blue solid line) for the 50 meter depth seismometer of station G39. The HVBW is taken as the mean over 5 teleseismic phases (Table 1)

.

7.2 Ellipticity Forward Modeling

Next to body-wave forward modeling, we apply a forward modeling tool for surface waves (Rayleigh waves) to further investigate the wave field composition. Rayleigh waves exhibit an elliptical particle motion confined to the radial-vertical plane (Aki and Richards, 2002). Many studies have shown that the H/V ratio of ambient noise is related to the amplitude ratio of the radial component of the Rayleigh wave over its vertical component (Arai and Tokimatsu, 2004; Bard, 1999; Bonnefoy-Claudet et al., 2006a; Konno and Ohmachi, 1998; Lachetl and Bard, 1994; Maranò et al., 2012, 2017) and that the H/V ratio does not depend on the source or the path of the Rayleigh wave, but it depends only on the structure beneath the receiving station (Ferreira and Woodhouse, 2007a, b). Rayleigh-wave ellipticity is frequency dependent in case of a layered and more complex subsurface. In case of a strong impedance contrast of factor 2.5-3.0, the ellipticity curve shows singularities where either the vertical or horizontal component vanishes (Wathelet, 2005). In theory, this results in a singular peak at the fundamental resonance frequency and a singular trough at higher frequency (Bard, 2002; Malischewsky and Scherbaum, 2004; Malischewsky et al., 2006). In reality, no full singularities are obtained since the recordings rarely contain pure Rayleigh waves.

The acquired subsurface shear-wave velocity profiles (Section 5) based on teleseismic arrivals, are used as input for Rayleigh-wave forward modelling, using the module Gpell in Geopsy (Wathelet et al., 2008). Velocities from the half-space (Chalk Group) are derived by averaging sonic logs from the wells Zeerijp and Borgsweer (Kruiver et al., 2017), which are assumed to

be constant over the area. We perform several tests to investigate the sensitivity for properties of the reference horizon (Malischewsky and Scherbaum (2004)), shear- and pressure wave velocity variations, single -and multiple velocity layers over a half space, and the presence of a high velocity layer representing the Brussel Sand Member. These variations are of minor impact on the resulting ellipticity curves.

Since instrument noise is dominating in the frequencies below 0.2 Hz, the fundamental peak of the ellipticity curves cannot be compared to the HVAN of the seismometers in the G-network. According to Maranò et al. (2012), the ellipticity ratio H/V of the fundamental mode does not only exhibit a peak at the fundamental resonance frequency (f_0), but also a trough at higher frequencies corresponding to the vanishing of the horizontal component. In the HVAN curve, a trough is well expressed and can be linked to the trough of the ellipticity fundamental mode while the first and second higher modes are hidden in the wide peak around 0.4 Hz and cannot be distinguished as single peaks in the HVAN (Fig.13a).

The misfit between the troughs of the fundamental-mode HVAN and modeled ellipticity is presented in Fig. 13(b). The majority of the stations are within the ≤ 0.03 Hz error range. The mean misfit is about zero, which indicates that the computation of HVBW and the further extraction of velocity profiles (Section 5) has not introduced a bias. From the overall good fit between the HVAN curves and ellipticity troughs of the fundamental mode, we can conclude that the input subsurface shear-wave velocity model is on average consistent with the measured ellipticity troughs of HVAN.

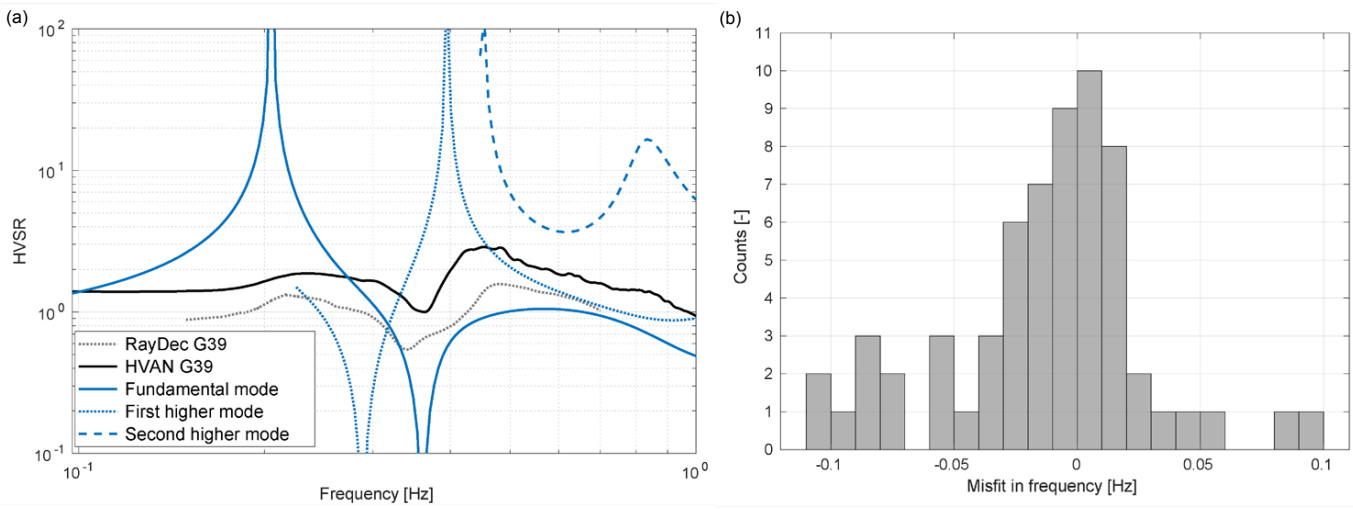

Figure 13. For all stations, the difference is determined between the trough of the HVAN at low frequencies and the negative singularity of the fundamental mode of the Rayleigh ellipticities. (a) Example of Rayleigh wave ellipticity curve for fundamental mode (blue line), first higher mode (dotted blue line) and second higher mode (dashed blue line), HVAN curve (black line) and RayDec (grey dotted line) for station G39. (b) Misfit between the troughs of the modeled ellipticity and the HVAN for all stations in the G-network.

Hobiger et al. (2009) developed RayDec, a method enabling Rayleigh-wave ellipticity to be extracted from the ambient noise based on the random decrement technique. We applied this method and compared the result with the HVAN curve and modeled ellipticity curves. In RayDec, the signal of each time window is projected in the direction of dominant polarization. This azimuth depends on the time-varying and frequency-dependent noise field. Thus, for a successful application of RayDec it is necessary to use small time windows and split up the larger frequency band in different bins. For site G39, the RayDec curve does show a trough close to the HVAN minimum (13a), therefore this technique confirms that this trough can be attributed to Rayleigh-wave ellipticity.

7.3 Ambient noise field composition

Body-wave (Fig. 12) and surface-wave (Fig. 13) forward modelling results are compared with HVAN to determine the ambient wave-field composition. It can be noted that there is a small offset in peak frequency between the shear-wave resonance peak for body waves (close to 0.19 Hz) and the ellipticity peak for surface waves (around 0.2 Hz). With an impedance contrast around factor 2.5-3.0 between the NSG and Chalk Group, the offset between the fundamental resonance frequency and ellipticity notch is consistent with the observations from Wathelet (2005). The HVAN (black line in Fig. 12) shows large similarity with the HVBW observed at G39 (blue line) between 0.4 and 1.0 Hz. This indicates that there is a prominent body-wave presence in the ambient noise, for the investigated frequency range, which corresponds with findings of Spica et al. (2018a). At the same time, there is a surface-wave presence, because Fokker and Ruigrok (2019) retrieved Rayleigh waves in this band, using noise recordings from the G-network.

The trough between 0.2 and 0.4 Hz can be seen both on the HVAN. This trough is not well developed in the modeled shear-wave resonance (gray dashed line in Fig. 12). It shows more similarities with the notch in the ellipticity (blue line in Fig. 13). With RayDec it was confirmed that there is indeed a Rayleigh-wave presence in this frequency band. This observation is supported by Kimman et al. (2012), who used a broad-band array in the Groningen area and found well-pickable phase velocities for Rayleigh waves between 0.2 and 0.4 Hz. Interestingly, a similar ellipticity trough can be seen in the HVAN (Fig. 12). This means that there must also be a (minor) contribution of Rayleigh waves in the teleseismic phases, in order to explain a similar notch. Direct Rayleigh waves will be largely attenuated at 0.3 Hz over teleseismic distances. Thus, the Rayleigh wave presence is likely in the coda of S-phases, due to conversions in or near the sedimentary sequence.

8 Discussion

In this paper we present a method to establish a shear wave-velocity profile for the North Sea Group (NSG) sedimentary layer, based on 5 teleseismic events at each station location of the Groningen borehole network. Subsequently, velocity profiles for the lower part of the NSG are constructed. These velocity profiles are used as input for body- and surface-wave forward modeling and compared to the H/V spectral ratios of the ambient noise (HVAN) to determine the wave-field composition. Moreover, we have validated the new shear-wave velocity profiles by comparing HVAN curves to the theoretical Rayleigh-wave ellipticity curves in the band where Rayleigh waves dominate. On average, there is a good match between the two. However, locally there

are inconsistencies between the HVAN and HVBW results. In this section we make a comparison with the existing velocity model of Deltares-NAM and discuss uncertainties and limitations of our approach.

The new shear-wave velocity profile for each station location is compared with the Deltares-NAM model (Fig. 14), which is constructed using fixed V_p/V_s ratios over the Groningen area and thus local lithological variations that affect the V_s differently than V_p are not accounted for. By using direct measurements of teleseismic phases per station, local subsurface variations are directly translated into average shear-wave velocities, which can explain the differences in velocities between the Deltares-NAM model and our model. The mean shear-wave velocity difference between the two models is -48 m/s. This negative mean difference means that HVBW derived velocities are in general higher than the Deltares-NAM velocities. The majority of the stations have less than 100 m/s difference in shear-wave velocity between the two models. Stations G58 and G59 represent the highest misfit in velocities because of the exceptional high V_s^{NSG} that we found.

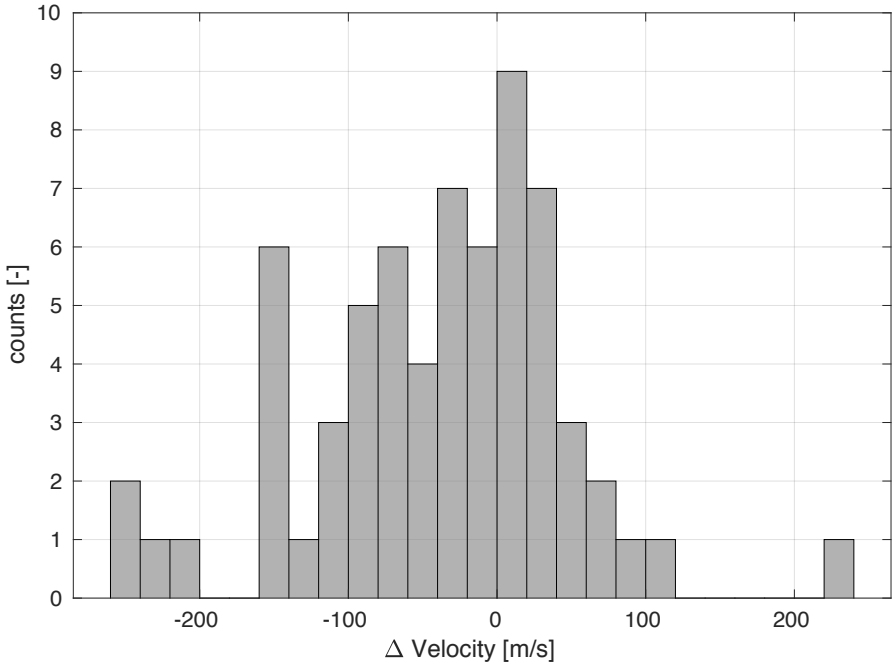

Figure 14. Histogram of the misfit between the Deltares-NAM velocity model (Kruiver et al. (2017)) and the velocity profiles for the lower part of the North Sea Group (V_s^{NSL}) presented in this paper. A count with a positive misfit corresponds to a station location with higher velocities in the Deltares-NAM model.

As for most unconsolidated sediments, in Groningen the V_s increases with depth, which results in surface waves showing their normal dispersive behavior, meaning that lower frequencies propagate faster. When Eq. 4 is used for finding the depth of these normally dispersive sediments, Bignardi (2017) showed that the depth is underestimated. Also we found, when modelling the resonance of a complex Groningen NSG model (Fig. 4), that f_0 is larger than in case of a single layer with the same

harmonic average as the sequence of layers. In the normally dispersive multilayer case, the part of the wave field that already reflects before reaching the free surface, interferes with the free surface reflection, leading to an increase of the combined f_0. The shift of f_0 is small and highly dependent on the near-surface model that is assumed. Nevertheless, using Eq. 4, a larger f_0 results in underestimation of the depth. Similarly, using Eq. 4 for finding an average V_s when the depth is known, a larger f_0 leads to an overestimation of the velocity. This finding is consistent with the —on average– overestimation of the velocity that we obtain with respect to the Deltares-NAM model.

Other assumptions that underlie Eq. 4 are that there are no losses and vertically incident body waves. Though f_0 goes up for a more realistic layering, f_0 goes down again when realistic losses are added to the model. Moreover, f_0 would further be reduced if a correction was made for the non-vertical incidence of the teleseismic phases, which were used for computing the HVBW. Since the exact corrections are unknown, it is not straightforward to make these corrections. On average we measure higher shear-wave velocities than the Deltares-NAM model, and this inconsistency might imply the dominant effect of multi-layer interference that is not incorporated in this model.

Finally, it has been assumed that a local 1D approximation can be made. The main impedance contrast is the base of the NSG, which is laterally smoothly varying over the region. This supports a local 1D assumption for each individual borehole station. Two stations at flanks of salt domes have been excluded from the analysis because of possible 3D effects.

In the near future, the updated V_s model will be tested for hypocentre localisation with the Groningen network. Because of the above considerations, it is expected that there is a bias in the absolute values, but that the lateral variations of V_s are quite well resolved.

9 Conclusions

In this paper, we have shown how average shear-wave velocities (V_s^{NSG}) of the soft sediments of the North Sea Group (NSG) can be retrieved from processing five teleseismic events for almost all stations of the Groningen network in the Netherlands. Average velocities for the lower part (V_s^{NSL}) were derived from the V_s^{NSG} and from detailed velocity profiles from the upper 200m. shear-wave velocities in the Lower NSG have a mean of 637 m/s, with local variations in a range from 465 m/s till 870 m/s.

The shear-wave velocities derived with teleseismic body-wave horizontal-to-vertical spectral ratio (HVBW) approximate the velocities in the Deltares-NAM model and show that this method is suitable for a first estimate of a shear-wave velocity model for an entire sedimentary sequence. Furthermore the new model has the advantage that it is derived from 63 direct site measurements and incorporates local subsurface variations. However, we are aware of limitations in our approach since we did not include a detailed layered subsurface model or attenuation and assumed vertical wave incidence. Therefore, the lateral variation we found is likely close to the actual variability over the boreholes. However, there could remain a bias in the absolute numbers. More generally, since many seismic properties are combined and partly interfering into a single spectrum,

the inversion of H/V curves is highly non-unique, no matter which underlying assumptions one puts in. Therefore, its main use is limited to the exploration stage.

Besides, the retrieved H/V curves from a month of ambient noise recordings were combined with Rayleigh ellipticity forward models. These forward models were based on shear-wave velocity profiles constructed from teleseismic phases. We have shown that the retrieved ellipticity curves from these input velocities are in good agreement with the horizontal-to-vertical spectral ratio of ambient noise (HVAN) curves.

In order to interpret stable resonance peaks, we computed the H/V ratios from the power spectrum densities, and subsequently computed probability density functions of the H/V ratios. With the permanent deployment of the Groningen network we were able to select the optimal duration of ambient noise recordings. We found that one month of data is sufficient to find a stable distribution for the resonance frequencies observed below 1.0 Hz.

For better understanding of the ambient wave-field composition, we performed Rayleigh-wave ellipticity forward modelling and shear-wave resonance forward modelling. By comparison of the HVAN and HVBW curves from the real data with the synthetic models, we found the presence of both body wave and surface waves in the ambient noise field in the low frequency range.

The method to derive average shear-wave velocities from teleseismic arrivals, from ambient noise, or a combination of the two as demonstrated in this paper, is confirmed as a powerful geophysical tool for exploring shear-wave velocities in a sedimentary layer. We have shown that strong teleseismic arrivals are useful in extending the frequency range in which resonance spectra can be found. Furthermore, we used the accurate mapping of sediment thickness over Groningen, together with the observed resonance frequencies, to find an empirical relation between the two. This relation can be used in other areas in the Netherlands where detailed depth maps are not available.

Code and data availability. Supplementary information is available on shear wave velocities for each borehole site and corresponding Matlab code to plot the velocity profile for each site

Author contributions. Janneke van Ginkel: constructed the manuscript with input from all co-authors, executed the H/V analysis and forward modeling. Elmer Ruigrok: daily advisor, developed PSD and PDF method, performed synthetic analysis, performed text input. Rien Herber, promotor, advisor, performed text corrections

Competing interests. No competing interests are present

Acknowledgements. This work is funded by EPI Kenniscentrum. Ambient noise and teleseismic phases were provided by KNMI and are publicly available through the website (http://rdsa.knmi.nl/dataportal). Information on global earthquakes was obtained from the EMSC

(https://www.emsc-csem.org). Figures are produced in Matlab, except Figure 2 is constructed in QGIS. We would like to thank Deltares and TNO for the use of their velocity models and subsurface data, and NAM for the data of the two reference boreholes Zeerijp and Borgsweer.

References

Aki, K. and Richards, P. G.: Quantitative Seismology, University Science Book, Sausalito, California, 2002.

Albarello, D. and Lunedei, E.: Combining horizontal ambient vibration components for H/V spectral ratio estimates, Geophysical Journal International, 194, 936–951, 2013.

Arai, H. and Tokimatsu, K.: S-wave velocity profiling by inversion of microtremor H/V spectrum, Bulletin of the Seismological Society of America, 94, 53–63, 2004.

Arai, H. and Tokimatsu, K.: S-wave velocity profiling by joint inversion of microtremor dispersion curve and horizontal-to-vertical (H/V) spectrum, Bulletin of the Seismological Society of America, 95, 1766–1778, 2005.

Bard, P.-Y.: Microtremor measurements: a tool for site effect estimation, The effects of surface geology on seismic motion, 3, 1251–1279, 1999.

Bard, P.-Y.: Extracting information from ambient seismic noise: the SESAME project (Site EffectS assessment using AMbient Excitations), European Project EVG1-CT-2000-00026 SESAME, 2002.

Bard, P.-Y., Campillo, M., Chavez-Garcia, F., and Sanchez-Sesma, F.: The Mexico earthquake of September 19, 1985—A theoretical investigation of large-and small-scale amplification effects in the Mexico City Valley, Earthquake spectra, 4, 609–633, 1988.

Bignardi, S.: The uncertainty of estimating the thickness of soft sediments with the HVSR method: A computational point of view on weak lateral variations, Journal of Applied Geophysics, 145, 28–38, 2017.

Bignardi, S., Mantovani, A., and Abu Zeid, N.: OpenHVSR: imaging the subsurface 2D/3D elastic properties through multiple HVSR modeling and inversion, Computers & Geosciences, 93, 103–113, 2016.

Bommer, J. J., Dost, B., Edwards, B., Stafford, P. J., van Elk, J., Doornhof, D., and Ntinalexis, M.: Developing an Application Specific Ground Motion Model for Induced Seismicity, Bulletin of the Seismological Society of America, 106, 158, https://doi.org/10.1785/0120150184, 2016.

Bommer, J. J., Stafford, P. J., Edwards, B., Dost, B., van Dedem, E., Rodriguez-Marek, A., Kruiver, P., van Elk, J., Doornhof, D., and Ntinalexis, M.: Framework for a ground-motion model for induced seismic hazard and risk analysis in the Groningen gas field, the Netherlands, Earthquake Spectra, 33, 481–498, 2017.

Bonnefoy-Claudet, S., Cornou, C., Bard, P.-Y., Cotton, F., Moczo, P., Kristek, J., and Donat, F.: H/V ratio: a tool for site effects evaluation. Results from 1-D noise simulations, Geophysical Journal International, 167, 827–837, 2006a.

Bonnefoy-Claudet, S., Cotton, F., and Bard, P.-Y.: The nature of noise wavefield and its applications for site effects studies: A literature review, Earth-Science Reviews, 79, 205–227, 2006b.

Bradley, B. A.: Strong ground motion characteristics observed in the 4 September 2010 Darfield, New Zealand earthquake, Soil Dynamics and Earthquake Engineering, 42, 32–46, 2012.

Chmiel, M., Mordret, A., Boué, P., Brenguier, F., Lecocq, T., Courbis, R., Hollis, D., Campman, X., Romijn, R., and Van der Veen, W.: Ambient noise multimode Rayleigh and Love wave tomography to determine the shear velocity structure above the Groningen gas field, Geophysical Journal International, 218, 1781–1795, 2019.

Dost, B., Ruigrok, E., and Spetzler, J.: Development of seismicity and probabilistic hazard assessment for the Groningen gas field, Netherlands Journal of Geosciences, 96, s235–s245, https://doi.org/10.1017/njg.2017.20, 2017.

Fäh, D., Kind, F., and Giardini, D.: A theoretical investigation of average H/V ratios, Geophysical Journal International, 145, 535–549, 2001.

Fäh, D., Kind, F., and Giardini, D.: Inversion of local S-wave velocity structures from average H/V ratios, and their use for the estimation of site-effects, Journal of Seismology, 7, 449–467, 2003.

Ferreira, A. M. and Woodhouse, J. H.: Source, path and receiver effects on seismic surface waves, Geophysical Journal International, 168, 109–132, 2007a.

Ferreira, A. M. and Woodhouse, J. H.: Observations of long period Rayleigh wave ellipticity, Geophysical Journal International, 169, 161–169, 2007b.

Fokker, E. and Ruigrok, E.: Quality parameters for passive image interferometry tested at the Groningen network, Geophysical Journal International, 218, 1367–1378, 2019.

Havskov, J. and Alguacil, G.: Instrumentation in earthquake seismology, vol. 358, Springer, 2004.

Hobiger, M., Bard, P.-Y., Cornou, C., and Le Bihan, N.: Single station determination of Rayleigh wave ellipticity by using the random decrement technique (RayDec), Geophysical Research Letters, 36, 2009.

Hofman, L., Ruigrok, E., Dost, B., and Paulssen, H.: A shallow seismic velocity model for the Groningen area in the Netherlands, Journal of Geophysical Research: Solid Earth, 122, 8035–8050, 2017.

Ibs-von Seht, M. and Wohlenberg, J.: Microtremor measurements used to map thickness of soft sediments, Bulletin of the Seismological Society of America, 89, 250–259, 1999.

Kimman, W., Campman, X., and Trampert, J.: Characteristics of seismic noise: fundamental and higher mode energy observed in the northeast of the Netherlands, Bulletin of the Seismological Society of America, 102, 1388–1399, 2012.

KNMI: Netherlands Seismic and Acoustic Network, Royal Netherlands Meteorological Institute (KNMI), Other/Seismic Network, 10.21944/e970fd34-23b9-3411-b366-e4f72877d2c5, 1993.

Konno, K. and Ohmachi, T.: Ground-motion characteristics estimated from spectral ratio between horizontal and vertical components of microtremor, Bulletin of the Seismological Society of America, 88, 228–241, 1998.

Kruiver, P. P., van Dedem, E., Romijn, R., de Lange, G., Korff, M., Stafleu, J., Gunnink, J. L., Rodriguez-Marek, A., Bommer, J. J., van Elk, J., et al.: An integrated shear-wave velocity model for the Groningen gas field, the Netherlands, Bulletin of Earthquake Engineering, pp. 1–26, doi: 10.1007/s10518-017-0105-y, 2017.

Lachetl, C. and Bard, P.-Y.: Numerical and theoretical investigations on the possibilities and limitations of Nakamura's technique, Journal of Physics of the Earth, 42, 377–397, 1994.

Lermo, J. and Chavez-Garcia, F. J.: Site effect evaluation using spectral ratios with only one station, Bulletin of the seismological society of America, 83, 1574–1594, 1993.

Lontsi, A. M., Sánchez-Sesma, F. J., Molina-Villegas, J. C., Ohrnberger, M., and Krüger, F.: Full microtremor H/V (z, f) inversion for shallow subsurface characterization, Geophysical Journal International, 202, 298–312, 2015.

Lunedei, E. and Malischewsky, P.: A review and some new issues on the theory of the H/V technique for ambient vibrations, in: Perspectives on European Earthquake Engineering and Seismology, pp. 371–394, 2015.

Malischewsky, P. G. and Scherbaum, F.: Love's formula and H/V-ratio (ellipticity) of Rayleigh waves, Wave motion, 40, 57–67, 2004.

Malischewsky, P. G., Lomnitz, C., Wuttke, F., and Saragoni, R.: Prograde Rayleigh-wave motion in the valley of Mexico, Geofísica internacional, 45, 149–162, 2006.

Maranò, S., Reller, C., Loeliger, H.-A., and Fäh, D.: Seismic waves estimation and wavefield decomposition: application to ambient vibrations, Geophysical Journal International, 191, 175–188, 2012.

Maranò, S., Hobiger, M., and Fäh, D.: Retrieval of Rayleigh wave ellipticity from ambient vibration recordings, Geophysical Journal International, 209, 334–352, 2017.

McNamara, D. E. and Buland, R. P.: Ambient noise levels in the continental United States, Bulletin of the seismological society of America, 94, 1517–1527, 2004.

Meijles, E.: De ondergrond van Groningen: een geologische geschiedenis, NAM, 2015.

Mulders, F. M. M.: Modelling of stress development and fault slip in and around a producing gas reservoir, TU Delft, Delft University of Technology, 2003.

Nakamura, Y.: A method for dynamic characteristics estimation of subsurface using microtremor on the ground surface, Railway Technical Research Institute, Quarterly Reports, 30, 1989.

Nakamura, Y.: What Is the Nakamura Method?, Seismological Research Letters, 90, 1437–1443, 2019.

Nishitsuji, Y., Ruigrok, E., Gomez, M., and Draganov, D.: Global-phase H/V spectral ratio for delineating the basin in the Malargue Region, Argentina, Seismological Research Letters, 85, 1004–1011, 2014.

Noorlandt, R., Kruiver, P. P., de Kleine, M. P., Karaoulis, M., de Lange, G., Di Matteo, A., von Ketelhodt, J., Ruigrok, E., Edwards, B., Rodriguez-Marek, A., et al.: Characterisation of ground motion recording stations in the Groningen gas field, Journal of seismology, 22, 605–623, 2018.

Parolai, S., Bormann, P., and Milkereit, C.: New relationships between Vs, thickness of sediments, and resonance frequency calculated by the H/V ratio of seismic noise for the Cologne area (Germany), Bulletin of the seismological society of America, 92, 2521–2527, 2002.

Peterson, J.: Observations and modeling of seismic background noise, US Geological Survey Albuquerque, Technical Report. 93-322, 1-95, 1993.

Rodriguez-Marek, A., Kruiver, P. P., Meijers, P., Bommer, J. J., Dost, B., van Elk, J., and Doornhof, D.: A Regional Site-Response Model for the Groningen Gas Field, Bulletin of the Seismological Society of America, 107, 2067–2077, 2017.

Ruigrok, E., Campman, X., and Wapenaar, K.: Basin Delineation with a 40 Hour Passive Seismic Record, Bulletin of the Seismological Society of America, 102, 2165–2176, 2012.

Sánchez-Sesma, F. J., Rodríguez, M., Iturrarán-Viveros, U., Luzón, F., Campillo, M., Margerin, L., García-Jerez, A., Suarez, M., Santoyo, M. A., and Rodríguez-Castellanos, A.: A theory for microtremor H/V spectral ratio: application for a layered medium, Geophysical Journal International, 186, 221–225, 2011.

Scherbaum, F., Hinzen, K.-G., and Ohrnberger, M.: Determination of shallow shear wave velocity profiles in the Cologne, Germany area using ambient vibrations, Geophysical Journal International, 152, 597–612, 2003.

Spica, Z., Perton, M., Nakata, N., Liu, X., and Beroza, G.: Site Characterization at Groningen Gas Field Area Through Joint Surface-Borehole H/V Analysis, Geophysical Journal International, 2017.

Spica, Z., Nakata, N., Liu, X., Campman, X., Tang, Z., and Beroza, G.: The ambient seismic field at Groningen gas field: An overview from the surface to reservoir depth, Seismological Research Letters, 2018a.

Spica, Z., Perton, M., Nakata, N., Liu, X., and Beroza, G.: Shallow VS imaging of the Groningen area from joint inversion of multimode surface waves and H/V spectral ratios, Seismological Research Letters, 2018b.

Thabet, M.: Site-Specific Relationships between Bedrock Depth and HVSR Fundamental Resonance Frequency Using KiK-NET Data from Japan, Pure and Applied Geophysics, 176, 4809–4831, 2019.

Tsai, N.: A note on the steady-state response of an elastic half-space, Bulletin of the Seismological Society of America, 60, 795–808, 1970.

Tsai, N. and Housner, G.: Calculation of surface motions of a layered half-space, Bulletin of the Seismological Society of America, 60, 1625–1651, 1970.

Van Dalfsen, W., Doornenbal, J., Dortland, S., and Gunnink, J.: A comprehensive seismic velocity model for the Netherlands based on lithostratigraphic layers, Netherlands Journal of Geosciences, 85, 277, 2006.

van Thienen-Visser, K. and Breunese, J.: Induced seismicity of the Groningen gas field: History and recent developments, The Leading Edge, 34, 664–671, 2015.

Vos, P.: Origin of the Dutch coastal landscape: long-term landscape evolution of the Netherlands during the Holocene, described and visualized in national, regional and local palaeogeographical map series, Barkhuis, 2015.

Wathelet, M.: Array recordings of ambient vibrations: surface-wave inversion, PhD Dissertation, Liége University, 161, 2005.

Wathelet, M., Jongmans, D., Ohrnberger, M., and Bonnefoy-Claudet, S.: Array performances for ambient vibrations on a shallow structure and consequences over Vs inversion, Journal of Seismology, 12, 1–19, 2008.

Wong, T. E., Batjes, D. A., and de Jager, J.: Geology of the Netherlands, The Publishing House of the Royal Netherlands Academy of Arts and Sciences, 2007.

Zhu, C., Cotton, F., and Pilz, M.: Detecting Site Resonant Frequency Using HVSR: Fourier versus Response Spectrum and the First versus the Highest Peak Frequency, Bulletin of the Seismological Society of America, 2020.